IEEE Access
Multidisciplinary | Rapid Review | Open Access Journal

Received January 26, 2019, accepted February 21, 2019, date of publication March 5, 2019, date of current version March 20, 2019.

Digital Object Identifier 10.1109/ACCESS.2019.2902949

Long Short-Term Memory Networks Based Automatic Feature Extraction for Photovoltaic Array Fault Diagnosis

ALBERT YAW APPIAH[1,2], XINGHUA ZHANG[1], BEN BEKLISI KWAME AYAWLI[1,3], AND FRIMPONG KYEREMEH[1,2]

[1]College of Electrical Engineering and Control Science, Nanjing Tech University, Nanjing 211816, China
[2]Department of Electrical/Electronic Engineering, Sunyani Technical University, Sunyani 233, Ghana
[3]Department of Computer Science, Sunyani Technical University, Sunyani 233, Ghana

Corresponding author: Albert Yaw Appiah (appibert@yahoo.com)

ABSTRACT Photovoltaic (PV) array fault diagnosis is important because it helps reduce energy and revenue losses to PV system operators. It also reduces fire hazards and electric shocks caused by PV array faults. As a result, many machine-learning-based fault diagnosis techniques have been proposed in recent times. Although the fault diagnosis accuracies associated with these techniques have been impressive, most machine learning algorithms rely on manual feature extraction, which is time consuming, expensive, and diagnostic expertise exacting. To address the problem of manual feature extraction, this paper proposes a new PV array fault diagnosis technique capable of automatically extracting features from raw data for PV array fault classification. The proposed technique utilizes long short-term memory networks, which is a deep learning algorithm, for feature extraction. The extracted features feed into a softmax regression classifier for fault diagnosis. The proposed technique exhibits high fault diagnosis accuracies on both noisy and noiseless data. In addition, the results of the proposed technique compare favorably with those of other techniques. It can, therefore, be inferred from the results that the proposed fault diagnosis technique offers an effective approach to automatically extract useful features from raw data and thus remove the need for the manual feature extraction.

INDEX TERMS Automatic feature extraction, fault diagnosis, long short-term memory, photovoltaic array, softmax regression.

I. INTRODUCTION

In recent years, application of photovoltaic (PV) energy has received global attention due to some desirable features associated with PV systems: non-environmental pollution during operation [1], ease of installation [2], low maintenance cost [3], and globally free and renewable availability of solar energy resource. Consequently, global installed capacity of PV energy has increased in recent years. The global installed capacity for the year 2000, 2014 and 2017 were 1.3GW [4], 177GW [4], and 402GW [5], respectively. In spite of these admirable features and growth, PV systems have some challenges which include relatively high initial cost [6], low electric power conversion efficiency [6], dependency on environmental conditions [7], [8], and fault vulnerability [9]. The latter is the focus of this research.

In most PV system installations, the PV arrays, which serve as the electric power generating units, are installed in harsh outdoor environments. Such outdoor environments expose PV arrays to potential PV array fault-inducing agents such as lightning, partial shading, mechanical and thermal impacts on cable insulation. Known PV array faults include ground fault (GF), line-to-line fault (LLF), arc fault (AF), and hot spot fault (HSF) [10], [11]. PV array faults have the effect of causing energy and revenue losses to PV system operators, electric shock, and fire hazards. For example, authors of [12] have reported that a multi-point PV array GF resulted in a fire hazard at Bakersfield, CA. The authors further reported that a large PV plant, located in California, USA, was involved in a fire hazard caused by LLF. A study[13] in UK indicates that

The associate editor coordinating the review of this manuscript and approving it for publication was M. Jaya Bharata Reddy.

average annual energy loss in domestic PV systems caused by faults is 18.9%. To avoid these negative effects caused by PV array faults, various national electrical installation codes make it mandatory to install protective device(s) on PV system installations depending on installation size and location.

Overcurrent protective devices (OCPDs), ground fault detection and interruption (GFDI) fuses, and arc fault circuit interrupters (AFCIs) are the protective devices usually adopted for LLF, GF, and AF, respectively [9], [14]. These protective devices have fuses, designed to melt whenever fault current exceeds the fuse rating in order to isolate the fault. However, these protective devices are unable to detect PV array faults that are of lower fault current magnitude [12], [15]. According to [15], factors that influence PV array fault current magnitude are solar irradiance level, maximum power point tracker (MPPT), fault impedance, fault location, potential difference between fault points, blocking diodes, and fault degradation. Due to the possibility of having a fault undetected, it is useful to conduct periodic manual checks on PV arrays to identify any undetected fault. However, Chen *et al.* [16] reject such periodic manual checks. The authors claim such manual checks can be time consuming, inaccurate, and injurious to operators.

Inspired by the need to detect and isolate PV array faults irrespective of fault current magnitude, many online PV array fault diagnosis techniques have been proposed in recent years. These online diagnosis techniques focus on detection and classification of fault, and they can be categorized into conventional thresholding and machine learning techniques [16].

In the thresholding-based techniques, fault detection is based on a difference between a measured quantity and its corresponding predicted quantity. If the difference is greater than a given threshold, fault is considered to have occurred, otherwise no fault. Reported studies that are based on the thresholding technique include [17]–[21]. Although the thresholding based techniques are relatively simple to design, they may suffer the following setbacks: (1) they only detect fault occurrence but do not give fault identity, (2) they rely on maximum power point operation, so MPPT failure impairs their diagnosis performance, and (3) they are affected by errors in models used for predictions.

Machine learning (ML) based techniques, on the other hand, utilize historical data of faulty and normal samples to derive fault diagnosis models. Various ML algorithms such as artificial neural networks (ANN) [22], [23], probabilistic neural networks (PNN) [23], extreme learning machine (ELM) [16], support vector machine (SVM) [24], random forest (RF) [5], and semi-supervised learning (SSL) [25] have been explored in search for better fault diagnosis techniques. On the whole, these ML-based fault diagnosis techniques have yielded encouraging diagnosis results. However, majority of these techniques depend on manual feature extraction, which requires diagnostic expertise and strong knowledge of signal processing. Moreover, manual feature extraction is time consuming and expensive. For example, in [24], a multi-resolution signal decomposition technique was utilized to extract features serving as inputs to a two-stage SVM classifier for LLF. This feature extraction approach demands high proficiency in signal processing. Also, it is expensive due to multiple filter requirements. In another instance, reported in [16], manual features were extracted from current-voltage curves for kernel-based ELM fault diagnosis technique.

To address the problem of manual feature extraction, this paper proposes a new fault diagnosis technique capable of automatically extracting features from raw data for diagnosis of PV array faults. The proposed technique utilizes LSTM networks for the feature extraction, after which the features are fed into a softmax regression classifier for classification. The decision to explore LSTM networks, for the first time, to extract features for PV array fault diagnosis is motivated by recent applications of LSTMs in electric power system line trip fault prediction [26] and milling machine cutters health monitoring [27].

The rest of the paper is organized as follows: Section II presents a description of a PV system and its related faults. Algorithms utilized for the proposed fault diagnosis technique are presented in Section III. A framework of the proposed fault diagnosis technique is presented in Section IV. Experimental results and discussion are presented in Section V. Finally, Section VI provides a conclusion of the study.

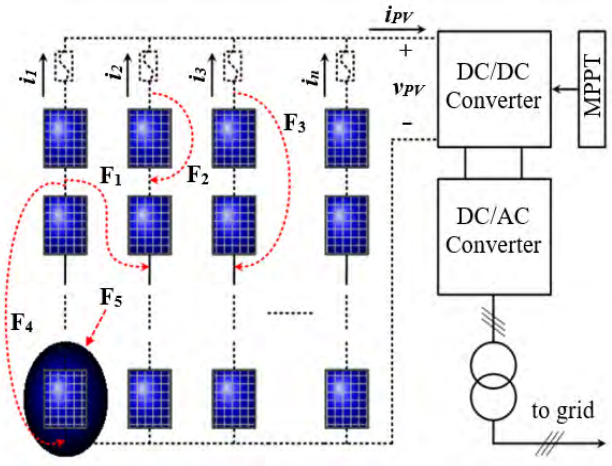

FIGURE 1. A typical configuration of a grid-connected PV system [24].

II. PV SYSTEM DESCRIPTION AND RELATED FAULTS

PV systems use one or more PV modules to generate electricity from incident solar irradiance. Based on applications, PV systems are broadly categorized into grid-connected and stand-alone systems. It is reported in [24] that grid-connected PV systems account for 95% of the world-wide installed PV capacity. Fig. 1 shows one of the most popular grid-connected PV system configurations. In addition to the PV modules, the grid-connected PV system is composed of direct current

to direct current (DC/DC) converter, maximum power point tracker (MPPT), a centralized direct current to alternating current (DC/AC) inverter, protective devices and auxiliaries. The MPPT ensures that the PV modules operate at their maximum power point (MPP) for efficient utilization of an available PV power. The MPPT does so by regulating the duty cycle of the DC/DC converter. The DC/AC converter converts the DC power coming from the PV modules into AC power in order to allow grid integration. Because no single PV module can generate electrical power sufficient for grid integration, multiple modules are generally configured in series-parallel fashion, which is generally referred to as PV array. A group of PV modules connected together in series form a PV array string.

Although several PV array fault types were introduced in section I, only LLF and HSF will be considered in the evaluation of the proposed fault diagnosis technique presented in section 4. For this reason, discussion of PV array faults is limited to these two. The decision to evaluate the proposed fault diagnosis technique on these two faults only is due to non-availability of data. Readers interested in comprehensive discussions of the various PV array faults can refer to [9].

- *LLF*: it is defined as an unexpected short circuiting between two points of different voltage potential in a PV array [28]. Cable insulation breakdown—which can be caused by water ingress, rodents, mechanical damage, and DC junction box corrosion—is the cause of LLF [24]. A LLF may occur within a PV array string (i.e. intra-string) or across different PV array strings (i.e. inter-string). As illustrated in Fig. 1, F_1 and F_2 are examples of inter and intra-string faults, respectively. The severity of an LLF is usually denoted as percentage mismatch, and it indicates the number of PV modules involved in the fault. Given that each string of Fig.1 contains 10 PV modules, F_1 and F_2 have 10% mismatch each. Alike, F_3 and F_4 have percentage mismatches of 20% and 90%, respectively. The higher the percentage mismatch the higher the fault current and vice versa. The impedance of the fault path is another factor which determines severity of an LLF.
- *HSF*: it is caused by partial or complete shading of PV modules. As shown in Fig. 1, F_5 points to a PV module which is assumed to be partially shaded. In such situation, the electrical characteristics of the shaded and unshaded modules become mismatched. The mismatch imposes a string current which reverse bias the shaded module. As a result, the shaded module begins to dissipate power. At a sufficiently large power dissipation, heat is generated, which increases the localized cell temperature of the shaded module.

  Beyond a certain localized temperature, the cell of the shaded module can be damaged. This process of increasing the module temperature (due to either partial or complete shading) is known as hot spotting, and the corresponding cells of the PV module with a higher temperature constitute the hot spot. Conventionally, bypass diodes have been used to mitigate the effect of HSF. However, the presence of these diodes introduce multiple peaks in the PV array's power-voltage characteristic curve and as a result render most MPPTs ineffective [29]. The severity of HSF depends on the level of shading and duration.

III. RELATED ALGORITHMS FOR THE PROPOSED FAULT DIAGNOSIS TECHNIQUE

This section presents a brief introduction to recurrent neural network (RNN) and long short-term memory (LSTM), and softmax regression algorithms. Based on these algorithms, a fault diagnosis technique is proposed.

A. RECURRENT NEURAL NETWORKS AND LSTM

A recurrent neural network (RNN) is an advanced version of artificial neural networks (ANNs). RNNs are sequence-based models capable of establishing temporal correlations between past and present information [30]. An RNN permits information of historical inputs to be stored in the network's internal state, and thus take advantage of all available input information at the current time. Theoretically, this indicates that RNNs can learn the features of any length of time series. In practice, however, RNNs suffer gradient vanishing and explosion problems [31]. Gradient vanishing problem refers to exponentially fast decreasing of gradient norm to zero, which limits an RNN model's ability to learn long-term temporal correlations while gradient explosion refers to the exact opposite [30].

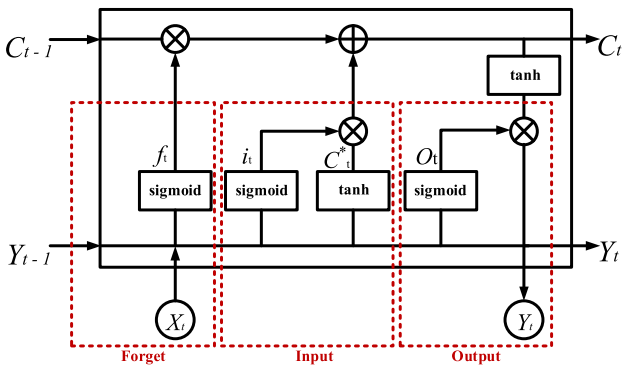

FIGURE 2. A single LSTM block containing a forget, input and output gates [33].

As a solution to the gradient vanishing problem faced by the RNNs, LSTM architecture has been proposed by Hochreiter and Schmidhuber [32]. Fig. 2 [33] presents a single LSTM block, which is composed of a memory cell represented as C_t and three gates: forget gate $f_t \in [0, 1]$, input gate $i_t \in [0, 1]$ and output gate $O_t \in [0, 1]$. Information flow through the LSTM block is handled by writing, erasing, and reading from the cell's memory state [34]. These operations are respectively handled by the input gate, forget gate, and output gate. The forget gate determines which information from the previous memory cell state has expired and so should be erased. The input gate selects information from

the candidate memory cell C_t^* to update the cell state. The output gate filters information from the memory cell so that the LSTM block considers only relevant information at its output.

The output values of each gate are computed using (1) [33], where $W_{[i,f,C,o]}$ are weight matrices and $b_{[i,f,C,o]}$ are bias vectors.

$$i_t = sigmoid\left(W_i * [Y_{t-1}, X_t] + b_i\right) \tag{1a}$$
$$f_t = sigmoid\left(W_f * [Y_{t-1}, X_t] + b_f\right) \tag{1b}$$
$$C_t^* = \tanh\left(W_c * [Y_{t-1}, X_t] + b_c\right) \tag{1c}$$
$$o_t = sigmoid\left(W_o * [Y_{t-1}, X_t] + b_o\right) \tag{1d}$$

The memory cell value C_t and the LSTM block output Y_t can be computed using (2), where $\odot$ stands for element-wise multiplication. For practical applications, a suitable number of LSTM blocks are combined to form a layer. Since, the LSTM does not suffer gradient vanishing problem, it has been adopted for the proposed fault diagnosis technique.

$$C_t = C_{t-1} \odot f_t + C_t^* \odot i_t \tag{2a}$$
$$Y_t = o_t \odot \tanh\left(C_t\right) \tag{2b}$$

B. SOFTMAX REGRESSION

Softmax regression is an extension of logistic regression for multiclass classification problems [35]. It is a supervised learning algorithm widely seen in deep learning architectures. A brief introduction to the algorithm is presented as follows: For a multiclass classification problem of K classes with M training samples denoted as $\left\{\left(x^{(i)}, y^{(i)}\right)\right\}_i^M$, where $y^{(i)} \in \{1, 2, \ldots, K\}$, the softmax regression estimates a probability $p\left(y = j|x\right)$ for each value of j $= 1, 2, \ldots,$ K. A formula for estimating the probabilities is given as (3) [36], [37].

$$p\left(y^{(i)} = j|x^{(i)}; \theta\right) = \frac{\exp\left(\theta_j^T x^{(i)}\right)}{\sum_{j=1}^{K} \exp\left(\theta_j^T x^{(i)}\right)} \tag{3}$$

In (3), θ is a matrix of parameters, which is defined in (4). θ_j is a column vector of parameters associated with the j^{th} class.

$$\theta = \begin{bmatrix} \theta_1^T \\ \theta_2^T \\ \cdot \\ \cdot \\ \cdot \\ \theta_K^T \end{bmatrix} \tag{4}$$

Through a gradient descent-based optimization algorithm, optimal values of θ can be determined by minimizing the cross-entropy loss expressed as (5) [35].

$$J\left(\theta\right) = -\frac{1}{M}\left[\sum_{t}^{N}\sum_{j}^{K} 1\left\{y^{(i)} = j\right\} \log \frac{\exp\left(\theta_j^T x^{(i)}\right)}{\sum_{j=1}^{K} \exp\left(\theta_j^T x^{(i)}\right)}\right] + \frac{\lambda}{2}\sum_{i}^{M}\sum_{j}^{K}\theta_{ij}^2 \tag{5}$$

where λ is a regularization parameter. The second term in (5) serves a purpose of regularization, which avoids variance problem. The classification rule of the softmax regression classifier for a test sample $x^{(i)}$ is given in (6).

$$y^{(i)} = \arg\max p\left(y^{(i)} = t|x^{(i)}; \theta\right) \quad t \in \{1, 2, \ldots K\} \tag{6}$$

IV. FRAMEWORK OF THE PROPOSED FAULT DIAGNOSIS TECHNIQUE

Fig. 3 is a workflow diagram, which provides a framework of the proposed fault diagnosis technique for PV array faults. First, input data are preprocessed. Next, features are automatically extracted from the preprocessed data for fault classification. Details of each stage in the work flow diagram together with a description of the utilized data are presented as follows:

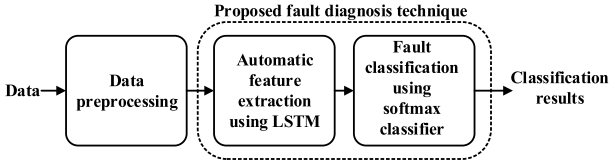

FIGURE 3. Workflow diagram of the proposed fault diagnosis technique.

A. DATA

Deep learning algorithms perform well when trained on sufficiently large data. Unfortunately, it is not practical to collect large field data (composed of faulty and normal samples) of arbitrary PV array operating conditions. This impracticability stems from the uncontrollable ambient temperature and solar irradiance of the PV array. Next, subjecting a real PV system installation to the faults considered in this paper can cause severe damages and safety hazards. For these reasons, the data utilized in this research were obtained via simulation. Details of the PV array system model used for data collection and a description of the collected data are presented as follows:

1) PV ARRAY SYSTEM MODELLING

Single-diode and double-diode are two popular models for PV cells [38]. Comparatively, the double-diode model offers better accuracy, but it is not seen as much as the single-diode model in literature. According to [39], a non-linear and implicit nature of the double-diode model hinder development of expressions for PV cell current-voltage characteristic. Fortunately, Matlab and Simulink software packages offer a PV array module, which is based on the single-diode module. To facilitate PV array simulation, the PV array module provided by Matlab and Simulink was adopted to build a 5.3 kW PV array system as shown in Fig. 4.

The gain blocks, shown in Fig. 4, were used to control the level of partial shading of the PV array modules. Table 1 presents standard test conditions (STC) parameter specifications of the PV module.

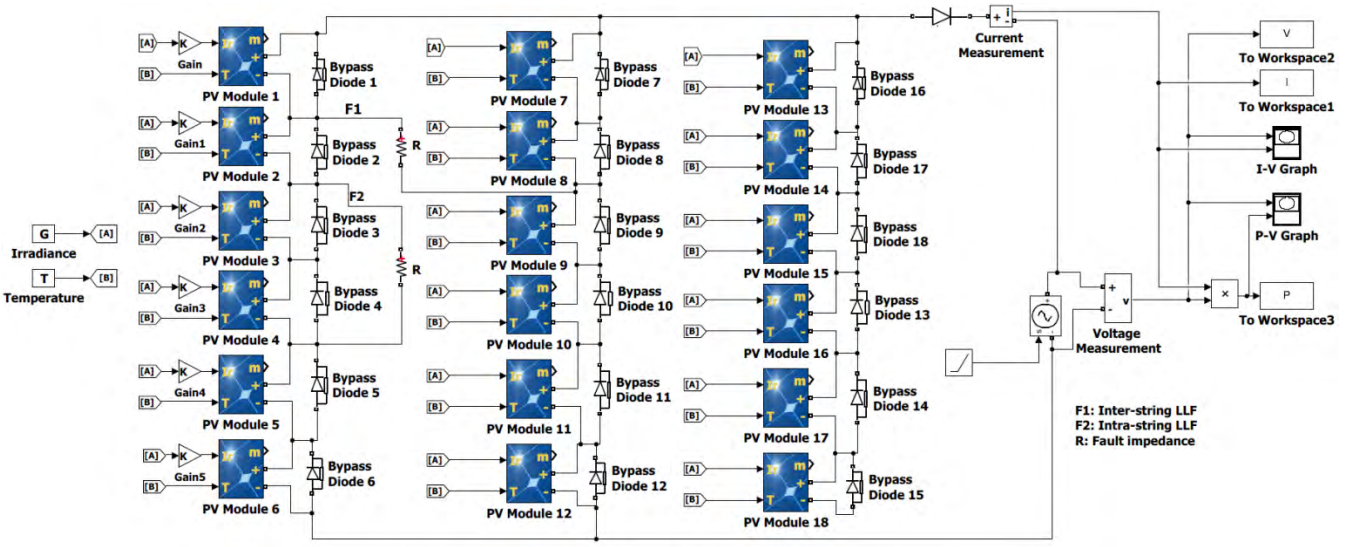

FIGURE 4. A 5.3 kW PV array system [24], [40].

TABLE 1. PV module parameters.

Items	Parameters	Specification
STC	Temperature	25 °C
	Irradiance	1000 W/m^2
PV Module	Maximum power (Pmax)	294.952 W
	Voltage at maximum power point (Vmp)	42.8 V
	Open circuit voltage (Voc)	50.93 V
	Short circuit current (Isc)	6.2 A

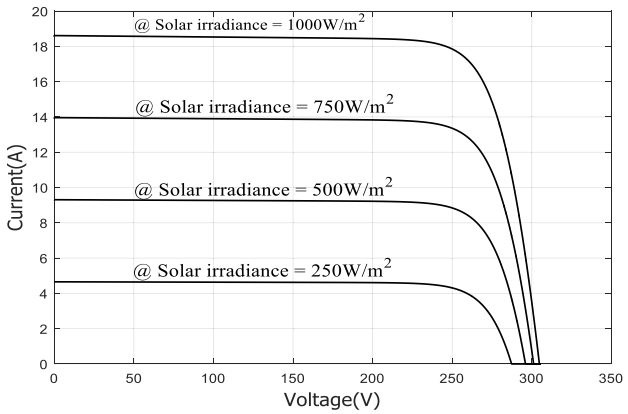

FIGURE 5. I-V characteristics of the PV array under normal operating conditions with ambient temperature of 25°C.

The model presented in Fig. 4 was utilized to simulate several instances of PV array normal and faulty operating conditions for data collection. Figs. 5, 6, and 7 respectively depict samples of current-voltage (I-V) characteristics for normal, LLF, and HSF conditions of the PV array. Fig. 5 shows that the PV array output current increases as solar irradiance increases and vice versa. This indicates that a PV array fault that occurs at a lower solar irradiance level will have lower fault current. From Fig. 6, we can observe

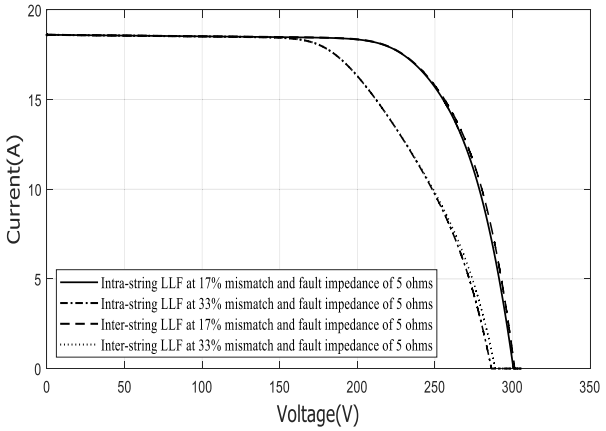

FIGURE 6. I-V characteristics of the PV array under LLF conditions.

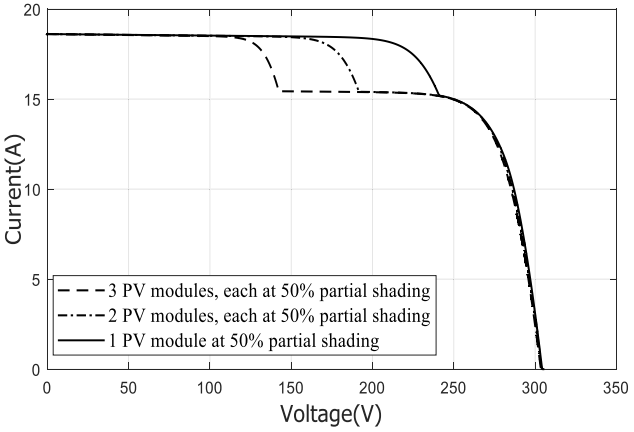

FIGURE 7. I-V characteristics of the PV array under HSF conditions.

that under same conditions, the open-circuit voltage of the PV array decreases with increase in fault mismatch level for both intra and inter-string LLFs. However, the short-circuit

current of the PV array remains unaffected. Finally, from Fig. 7, we observe that partial shading, which causes HSF, distorts the I-V characteristic of the PV array. This distortion gives rise to multiple maximum power points.

2) DATA DESCRIPTION

The PV array output current (I), voltage (V), and power (P) were selected, sensed and logged as data. The reason for using these variables is that an occurrence of any of the faults considered in this paper directly affects either I or V and indirectly affects P. Simultaneously, data samples of these variables were sensed and logged for each normal or faulty condition that was simulated. From each of the three variables (I, V, and P), 6067 data samples were collected and labelled. Each sample is a sequence of 400 data points. All samples from I were clustered as $I\_dataset$ and same was done for V and P to generate $V\_dataset$ and $P\_dataset$, respectively. The samples were obtained by simulation of the pv array with combinations of different temperatures, solar irradiance, fault impedances, percentages of partial shading, and LLF with different percentage mismatches. These combinations are representative of real world PV array operating conditions, and as a result make the data generated data realistic. Details of these combinations are presented as follows:

- Line-line fault: 2240 cases of LLF were simulated. These conditions originated from combinations of different PV array operating temperature (from 10°C to 40°C, at a step change of 5), different solar irradiance levels (from 100 W/m^2 to 1000 W/m^2, at step change of 100), different fault impedances (0, 5, 10, 15 Ω), and different mismatch percentages (16.7, 33.7, 50, 66)%. Both inter and intra-string LLFs were considered. It is worth noting that the initially low values of the solar irradiance considered in the simulations make it possible to create fault cases of low fault current magnitude, which may be uncleared by a conventional protective device such as OCPD. For example, an LLF occurring at a solar irradiance value of say 100W/m^2, 200W/m^2, or 300W/m^2 will have a low fault current magnitude.
- *Hot spot fault*: 1961 cases of HSF were simulated. Different partial shading levels (40, 50, 60, 70, 80, 90)% of PV modules within a PV string were considered. These shading cases were simulated along with different combinations of solar irradiance (from 500 W/m^2 to 1000 W/m^2, at a step of 50) and temperature (from 10°C to 35°C, at a step of 5).
- *Normal condition*: Since it is required of the fault diagnosis technique to distinguish between healthy and faulty conditions, data samples from a normal working PV array were collected as part of the data. Different combinations of PV operating temperature (5°C to 50°C with a step change of 5) and solar irradiance levels (55W/m^2 to 1000W/m^2, a step change of 50) were considered. A total of 1866 normal conditions were sampled.

3) NOISY DATA DESCRIPTION

The data described in subsection 2 were considered noiseless since it does not incorporate noise (i.e. disturbance). In real world situations, a certain level of noise is almost always present in a data acquired through sensing and measuring instruments. Hence, an attempt has been made to create a noisy data by adding noise to the noiseless data to reflect real world situations as close as possible. The noise signal generation approach, which was adopted from [23], is expressed in (7).

$$\text{Disturbance} = A + B \times randn(1, \text{N}) \tag{7}$$

where A denotes the mean of the disturbance signal, B is the amplitude of the disturbance signal, $randn()$ is a predefined Matlab noise function, and N is the size of the disturbance signal. The corresponding disturbances generated for the I, V, and P data samples were based on the following amplitudes: $B_{\text{I}} = 2\text{A}$, $B_{\text{V}} = 5\text{V}$ and $B_{\text{P}} = 5\text{W}$.

B. DATA PREPROCESSING

Data preprocessing is an important operation in both ML and DL algorithms to reduce the impact of different magnitudes and dimensions present in a given data and to increase convergence rate [26]. Therefore, all data samples were preprocessed with a 0-1 standardization. Using $I\_dataset$ as illustration, data preprocessing was implemented based on (8).

$$I_p^{(i)} = \frac{I^{(i)}}{\max\left(I\_dataset\right)} \tag{8}$$

where $I_p^{(i)}$ is a preprocessed version of the i^{th} data sample from $I\_dataset \in \mathbb{R}^{6067\times400}$ and $\max\left(I\_dataset\right)$ is the maximum element of $I\_dataset$. The division operation was carried out in element-wise fashion. As part of the preprocessing stage, the preprocessed data were divided into training, validation and testing data sets for experimental evaluation of the proposed fault diagnosis technique.

C. PROPOSED FAULT DIAGNOSIS TECHNIQUE

Fig. 8 illustrates a model for the proposed fault diagnosis technique, which handles both automatic feature extraction and fault classification. The LSTM and the softmax regression classifier, which were introduced in section III, respectively perform feature extraction and fault classification roles.

The number of time steps and input data size have influence on LSTM network's performance and complexity. Therefore, each LSTM network layer was designed to accommodate 25 LSTM blocks, where each block corresponds to a time step in the sequence data to be fed into the network. Since there are three PV array operating conditions to be classified, the softmax regression classifier was designed to have three output nodes. Detailed explanations of the feature extraction and the fault classification are presented next.

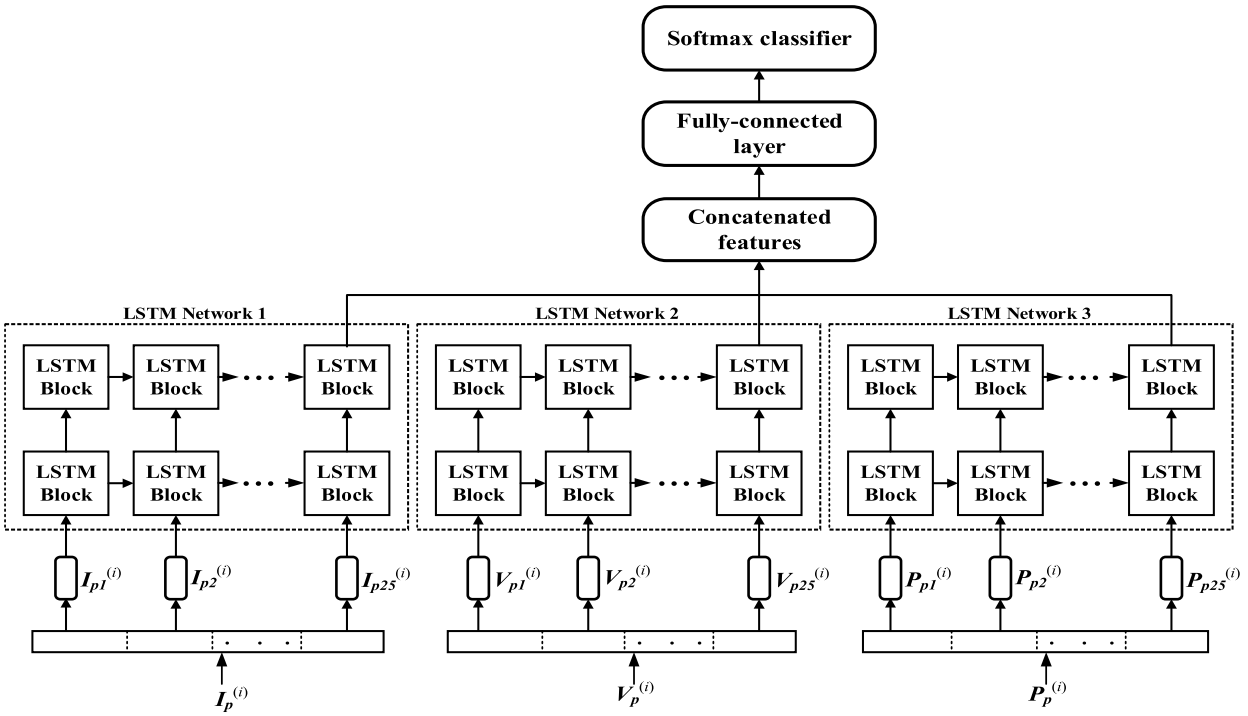

FIGURE 8. A model for the proposed fault diagnosis technique.

1) AUTOMATIC FEATURE EXTRACTION USING LSTM NETWORKS

Three LSTM networks were designed (Fig. 8) to extract useful features from the raw data sets. The LSTM network 1, 2, and 3, respectively extract features from the *I_dataset*, *V_dataset*, and *P_dataset*. Each of the preprocessed data samples, which is a 400-dimensional vector, was translated into 25 segments before being fed into its corresponding LSTM network. Each segment contains 16 data points and represents a time step in the raw sequence data. For instance, as shown in Fig. 8, $I_{p2}^{(i)}$ represents an input to the LSTM Network 1 at the 2nd time step.

The preprocessed and segmented sequential data samples get fed and propagated through the LSTM networks. As each given data sample propagates through the LSTM networks, the various LSTM blocks extract features from the sample through recurrent updates of their output activations using (2b). For clarity, (2b) is restated in a slightly different form as (9).

$$Y_t^l = \text{LSTM}\,(X_t, Y_{t-1}, \theta) \tag{9}$$

where l is the layer number of the network, and Y is the output activation of the LSTM block at time step t, and θ represents parameters associated with the LSTM block. In each output layer of the three LSTM networks, we consider the output of the LSTM block at the final time step T as the most useful feature representation of the input data. This decision is based on the fact that LSTM networks are able to capture long range interdependencies in a sequential data.

Given that each LSTM block of the three networks considered in Fig. 8 has n activations in its output layer L, the extracted features from LSTM Networks 1, 2, and 3 can be mathematically represented as shown in (10), (11) and (12) respectively. In order to feed the extracted features from the three LSTM networks into the softmax regression classifier, (10), (11) and (12) are concatenated as illustrated in (13). Fig. 9 illustrates a heatmap visualization of the features extracted by the LSTM networks from the raw data for NC, HSF, and LLF.

$$Y_t^{L<\text{LSTM Network 1}>} = \begin{bmatrix} a_1 \\ a_2 \\ \vdots \\ a_n \end{bmatrix} \in \mathbb{R}^{n\times 1} \tag{10}$$

$$Y_t^{L<\text{LSTM Network 2}>} = \begin{bmatrix} b_1 \\ b_2 \\ \vdots \\ b_n \end{bmatrix} \in \mathbb{R}^{n\times 1} \tag{11}$$

$$Y_t^{L<\text{LSTM Network 3}>} = \begin{bmatrix} c_1 \\ c_2 \\ \vdots \\ c_n \end{bmatrix} \in \mathbb{R}^{n\times 1} \tag{12}$$

$$\textit{Concatenated features} = \begin{bmatrix} Y_T^{L<\text{LSTM Network 1}>} \\ Y_T^{L<\text{LSTM Network 2}>} \\ Y_T^{L<\text{LSTM Network 3}>} \end{bmatrix} \in \mathbb{R}^{3n\times 1} \tag{13}$$

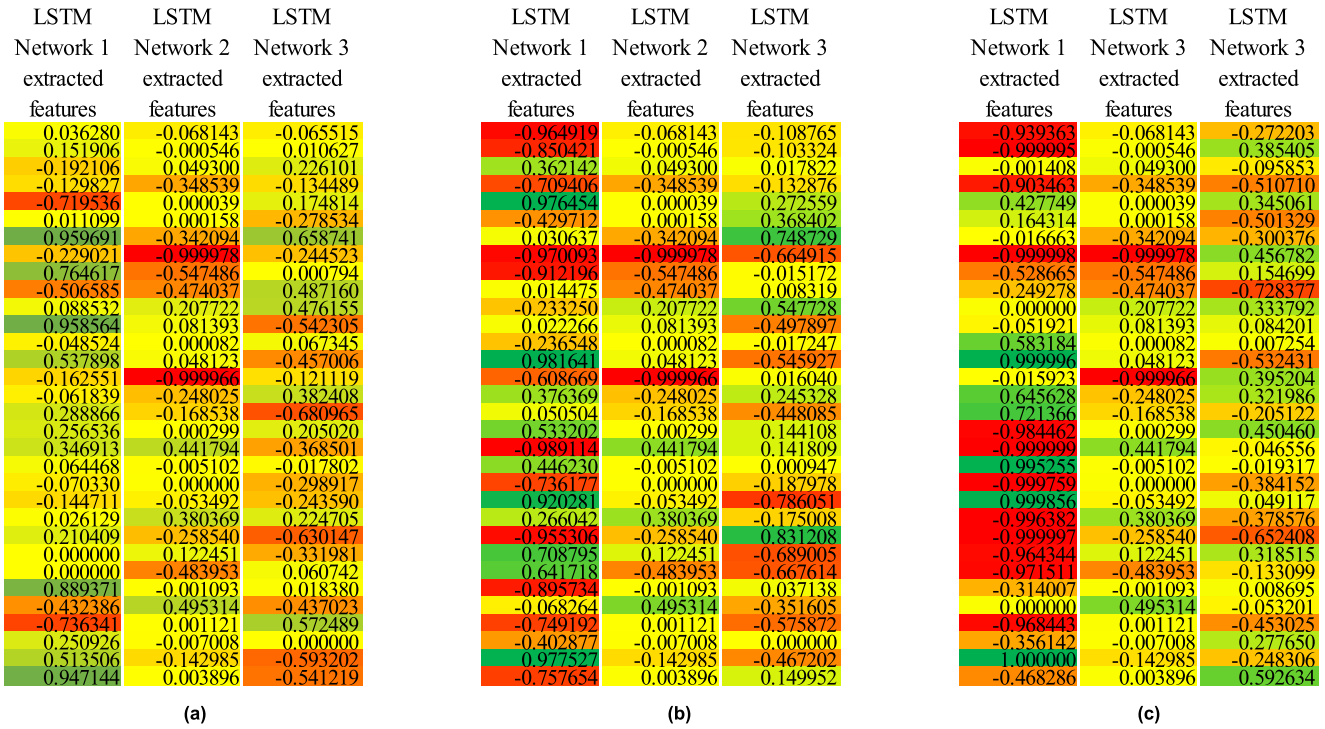

FIGURE 9. (a) Heatmap visualization of LSTM-network extracted features for NC, (b) Heatmap visualization of LSTM-network extracted features for HSF, (c) Heatmap visualization of LSTM-network extracted features for LLF.

2) FAULT CLASSIFICATION

The concatenated features pass through one fully-connected (FC) layer and finally to a softmax regression classifier for fault classification. The FC layer refines and compresses the concatenated features. For a given data sample, the softmax classifier estimates class probabilities from the concatenated feature using (3). Based on the classification rule presented in (6), the softmax regression classifier predicts the class label for the given data sample.

D. EXPERIMENTAL IMPLEMENTATION

An experimentation of the proposed fault diagnosis technique has been carried out in order to evaluate its performance. The computer used for the experiment is a desktop computer with Intel (R) Core (TM) i7-7700 @ 3.60 GHz central processing unit (CPU) with 16.0 GB RAM. The model of the proposed fault diagnosis technique was implemented with Keras library. Tensorflow was used as a backend to Keras. Keras is a deep learning framework based on Theano and Tensorflow, which supports both CPU and graphics processing unit (GPU) [41]. The framework is coded in Python programming language in a modular fashion. Several modules for implementing DL algorithms, optimizers and cost functions are included in Keras, which make quick implementation of the proposed technique possible.

The noiseless data, described in section IV, were partitioned into training, validation, and testing data sets with a ratio of 70:15:15, respectively. Using the training and validation data sets, the Keras-implemented model of the proposed technique was trained and validated based on the hyperparameters summarized in Table 2. Grid search method was utilized to obtain the hyperparameters, where several combinations of hyperparameter values were tried and the best combination adopted. Finally, the testing data set was utilized to test the performance of the trained model. Adaptive moment estimation (Adam) optimization algorithm was adopted for learning the parameters (weights and biases) associated with the model. The learning rate specifies the rate at which the parameters get updated during training. The batch size refers to the amount of training data used for one run of parameter updates. Hence, the lower the value, the more often a parameter gets updated and the more time is

TABLE 2. A summary of hyperparameters.

Hyperparameter	Value
Input time steps	25
Input feature dimension	16
Batch size	128
Learning rate	0.002
Adam optimizer	β_1=0.9, β_2=0.999
# Epochs	50
# nodes in each LSTM input layer	100
# nodes in LSTM output layer	32
# nodes in the FC layer	40
# nodes in the softmax layer	3

required for training the model. Epoch refers to one iteration through the entire training set.

V. EXPERIMENTAL RESULTS AND DISCUSSION

A. TRAINING AND VALIDATION RESULTS BASED ON THE NOISELESS DATA

The essence of training the model was to learn the model's associated parameters. Validation was used to perform error analysis, which helped to establish the presence or otherwise of bias and variance problems in the model. To help monitor training and validation performances, this paper adopted accuracy and loss as evaluation metrics. Accuracy is defined as a measure of a fraction or percentage of data samples whose labels were correctly predicted. Loss can be viewed as an error, and it measures how good the output of the model is compared with a ground truth label.

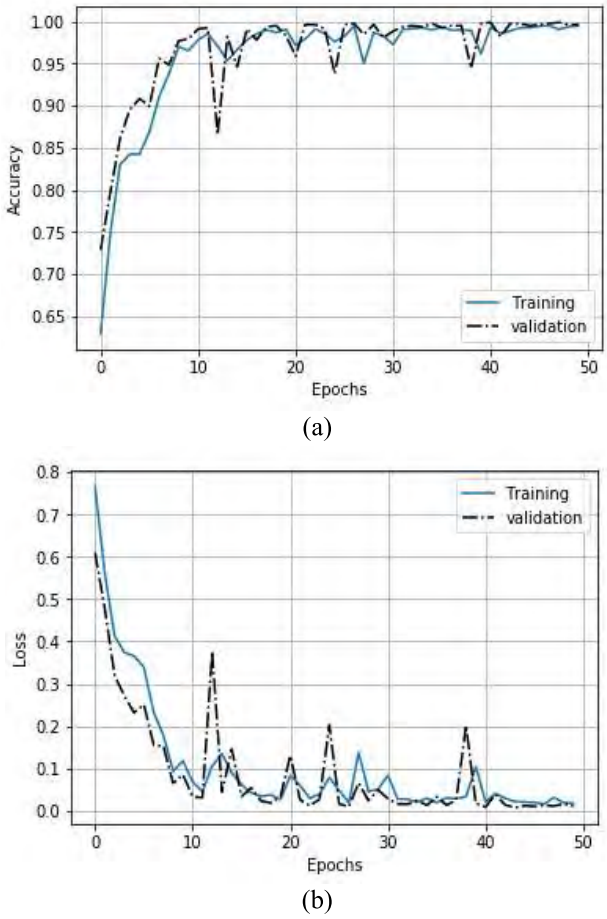

FIGURE 10. Convergence curves of the training process (a) Training accuracy versus. validation accuracy (b) training loss versus validation loss.

Fig. 10a shows plots of how both training and validation accuracies evolved over the training epochs, based on the noiseless datasets. By inspection, it can be noticed from Fig. 10a that the training accuracy gradually increases and converges around 99.06%.

This gradual increases in the training accuracy means that both the LSTM networks and the classifier parts of the proposed model learn much better optimized parameters over each epoch until convergence. The optimized parameters learned by the LSTM networks play a key role in the computation of the LSTM networks output values (i.e. activations). As previously mentioned, the concatenated outputs (activation values) of the three-LSTM networks serve as the automatically extracted features for fault diagnosis by the softmax classifier. The high training accuracy at convergence thus suggests that the LSTM networks are capable of automatically extracting features from the raw data. Again, as Fig. 10a shows, the simultaneous gradual increases in both training and validation accuracies give an indication that the trained model is not having a variance problem. This absence of a variance problem gives a high expectation that the model will generalize well on the testing data set. As an alternative way to view the training performance, the evolution of both training and validation losses over the epochs were plotted as shown in Fig. 10b. Since loss is a measure of error, the smaller the loss value at convergence, the better the model. At convergence, both training and validation loss were around 0.025.

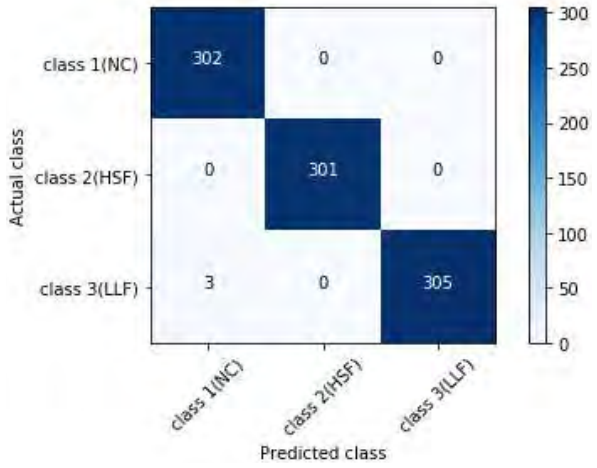

FIGURE 11. Fault classification results based on the noiseless data.

B. TESTING RESULTS BASED ON THE NOISELESS DATA

The LLF and HSF, which were considered in this paper, together with a normal condition (NC) of the PV array present a multi-class classification problem for the model of the proposed fault diagnosis technique. Fig. 11 is a classification results obtained from the model, presented in a confusion matrix. Entries of the confusion matrix are explained as follows. The sum of entries along a given row of the confusion matrix represents total number of testing dataset samples for a given class associated with the row.

The proposed fault diagnosis technique classified 302 testing data samples from class 1 as belonging to class 1; 3 testing data sample from class 3 as belonging class 1; 301 testing data samples from class 2 as belonging to class 2; 305 testing data samples from class 3 as belonging to class 3. From the

explanations given, it follow that the fault classification accuracies of the proposed fault diagnosis technique for NC, HSF, and LLF are 100%, 100% and 99.03% respectively (class accuracy = number of correct predictions for a the class/total number of class samples). These high levels of classification accuracies suggest that the proposed model will hardly raise a false fault alarm. Moreover, the almost 100% accuracy for the three classes indicates that the proposed model is capable of detecting faults irrespective of fault current magnitude.

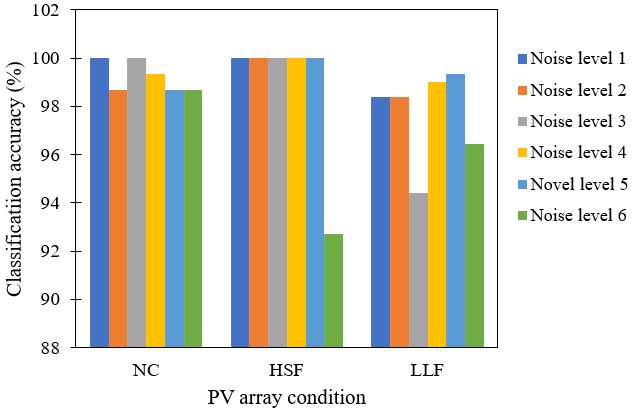

FIGURE 12. Fault classification results based on the noisy data at different noise levels.

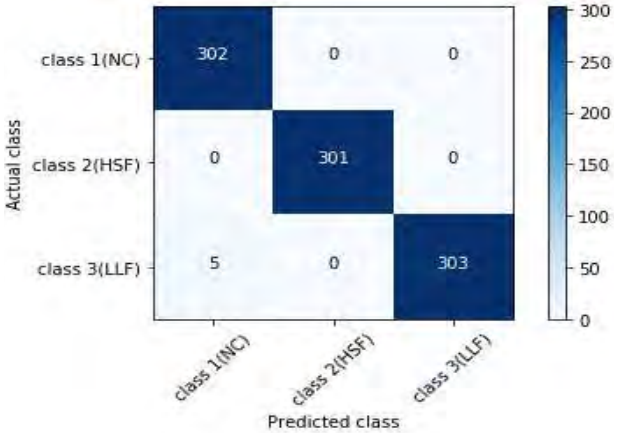

FIGURE 13. Fault classification results based on the noisy data at noise level 1 (Noise amplitudes: $B_I = 2A$, $B_V = 5V$, and $B_P = 5W$).

C. TESTING RESULTS BASED ON THE NOISY DATA

The proposed PV array fault diagnosis technique has also been trained and tested on the noisy data. Six different noise levels were considered. Fig. 12 presents a summary of results obtained on the noisy data. The detailed results from which this summary was derived are presented as an appendix to this paper (Figs. 13-18). With reference to Fig. 12, the following observations can made:

- For fault classification accuracy, the worst and best for NC are 98.68% and 100% respectively, and the average of all the six cases considered is 99.23%. Although not constant, the degradation in fault classification accuracy is mild.

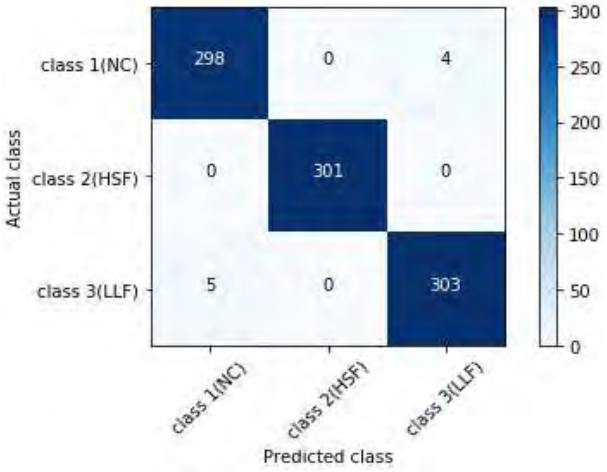

FIGURE 14. Fault classification results based on the noisy data at noise level 2 (Noise amplitudes: $B_I = 4A$, $B_V = 7V$, and $B_P = 7W$).

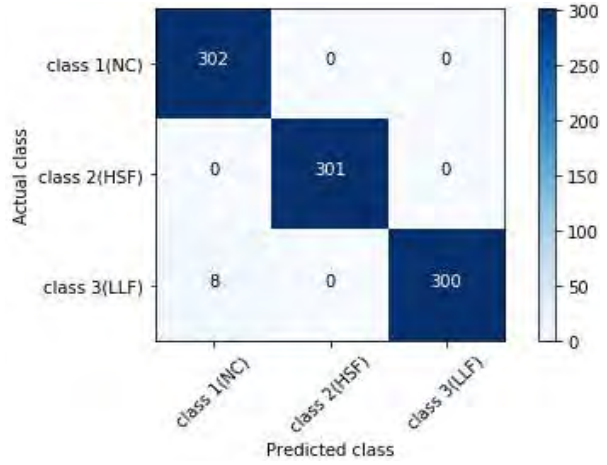

FIGURE 15. Fault classification results based on the noisy data at noise level 3 (Noise amplitudes: $B_I = 6A$, $B_V = 9V$, and $B_P = 9W$).

- For fault classification accuracy, the worst and best for HSF are 92.69% and 100% respectively, and the average of all six cases considered is 98.78%. Fault classification accuracy remains constant except at noise level 6, where there is a sharp decline.
- For fault classification accuracy, the worst and best for LLF are 94.40% and 99.35% respectively, and the average of all six cases considered is 97.66%. Contrary to the observations made for NC and HSF, there is a rise and fall in accuracy as the noise levels increase.

The evidence presented here supports a conclusion that our proposed fault diagnosis technique is robust to noise. We, however, wish to state that extremely high noise levels can degrade the performance of the technique proposed in this paper. Hence, quality sensors must be used for data acquisition in its real world implementation.

D. COMPARISON OF FAULT DIAGNOSIS TECHNIQUES

Although the objective of this research is to automatically extract useful features for PV array fault diagnosis, it is

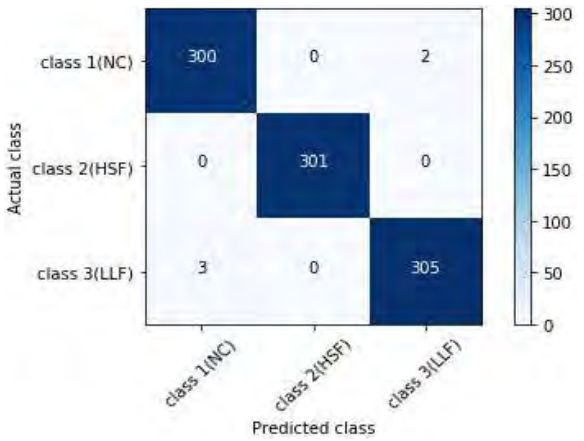

FIGURE 16. Fault classification results based on the noisy data at noise level 4 (Noise amplitudes: $B_I = 8A$, $B_V = 11V$, and $B_P = 11W$).

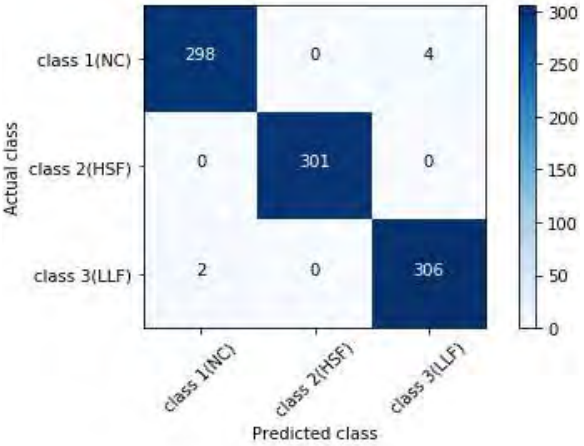

FIGURE 17. Fault classification results based on the noisy data at noise level 5 (Noise amplitudes: $B_I = 10A$, $B_V = 13V$, and $B_P = 13W$).

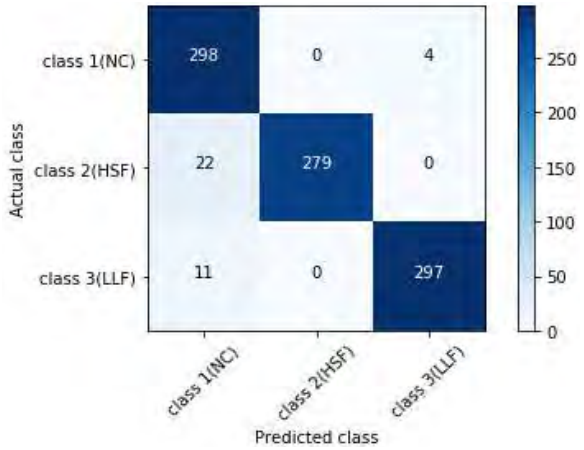

FIGURE 18. Fault classification results based on the noisy data at noise level 6 (Noise amplitudes: $B_I = 12A$, $B_V = 15V$, and $B_P = 15W$).

important not to achieve this noble objective at the expense of fault classification accuracy. Therefore, this section compares the fault classification results of the proposed fault diagnosis technique with those of three other techniques in order to see its relative performance. These other techniques are SVM [23], ANN [22] and PNN [22]. For brevity, our proposed technique is hereafter referred to as LSTM-based technique.

In [23], an SVM-based fault detection technique for LLF was presented, where six interesting cases of LLFs were considered. Worst and best case average fault classification accuracies reported are 40.42% and 96.67% respectively. The average accuracy of all six test cases evaluates to 77.57%. Although encouraging, it worth mentioning that these results were based on standard test conditions (STC), so the performance of the technique in many other operating conditions is not established. A limited number of partial shading cases were also detected with an accuracy of 100%. In [22], ANN and PNN based techniques have been reported. Performances of both techniques based on LLF and open circuit fault (OCF) have also been reported. In [22], a 3-module and 10-module intra-string short-circuit faults were created and code-named Fault #1 and Fault #2 respectively. Therefore, both faults have been reported as such in Table 3. Average fault classification accuracies reported for the ANN and PNN were deduced from the confusion matrices reported by the authors.

TABLE 3. Fault classification accuracies of the compared methods.

Techniques	Dataset description	Fault type	Fault classification accuracy (%)
LSTM-based technique	Noiseless (simulated)	NC	100.00
		HSF	100.00
		LLF	99.03
	Noisy (simulated)	NC	99.23
		HSF	98.78
		LLF	97.66
SVM [24]	Noiseless (simulated)	LLF	77.57
		HSF	100.00
ANN [23]	Noiseless (simulated)	LLF (Fault #1)	86.96
		LLF (Fault #2)	100.00
		OCF	32.61
	Noisy (simulated)	LLF (Fault #1)	69.02
		LLF (Fault #2)	91.85
		OCF	69.02
PNN [23]	Noiseless (simulated)	LLF (Fault #1)	100
		LLF (Fault #2)	100
		OCF	100
	Noisy (simulated)	LLF (Fault #1)	100.00
		LLF (Fault #2)	94.57
		OCF	100.00

Table 3 summarizes the results of the compared techniques. By and large, the LSTM-based technique competes well with the other techniques.

VI. CONCLUSION

Most ML-based PV array fault diagnosis techniques depend on manual feature extraction, which is time consuming, expensive, and diagnostic expertise demanding. To avoid this manual feature extraction, this paper has proposed a new PV array fault diagnosis technique. The proposed fault diagnosis technique combines LSTM networks and softmax

regression classifier. The LSTM networks function as an automatic feature extractor to extract features from the raw data. The features extracted by the LSTM networks feed into the softmax regression classifier for fault classification. A model of the proposed fault diagnosis technique has been trained, validated, and tested on both noisy and noiseless data sets composed of three conditions namely: normal condition (NC) line-to-line fault (LLF), and hot spot fault (HSF).

Fault classification accuracies of our proposed fault diagnosis technique, based on the noiseless data, for NC, HSF, and LLF are 100%, 100%, and 99.03%, respectively. In the case of a noisy data, the proposed technique demonstrated robustness to noise with average fault classification accuracies of 99.23%, 98.78%, and 97.66% for NC, HSF, and LLF, respectively. Based on these results, it can be concluded that the LSTM networks are effective for extracting features from the raw data for PV array fault diagnosis. Implementation of the proposed fault diagnosis technique can avoid the need for manual feature extraction.

APPENDIX

Figs. 13-18 present classification results obtained from the proposed PV array fault diagnosis technique based on noisy data at different noise levels.

REFERENCES

[1] L. L. Jiang and D. L. Maskell, "Automatic fault detection and diagnosis for photovoltaic systems using combined artificial neural network and analytical based methods," in *Proc. Int. Joint Conf. Neural Netw. (IJCNN)*, Killarney, Ireland, 2015, pp. 1–8.

[2] A. Mellit, G. M. Tina, and S. A. Kalogirou, "Fault detection and diagnosis methods for photovoltaic systems: A review," *Renew. Sustain. Energy Rev.*, vol. 91, pp. 1–17, Aug. 2018.

[3] M. Seyedmahmoudian *et al.*, "Simulation and hardware implementation of new maximum power point tracking technique for partially shaded PV system using hybrid DEPSO method," *IEEE Trans. Sustain. Energy*, vol. 6, no. 3, pp. 850–862, Jul. 2015.

[4] Z. Yi and A. H. Etemadi, "Fault detection for photovoltaic systems based on multi-resolution signal decomposition and fuzzy inference systems," *IEEE Trans. Ind. Electron.*, vol. 8, no. 3, pp. 1274–1283, May 2017.

[5] Z. Chen *et al.*, "Random forest based intelligent fault diagnosis for PV arrays using array voltage and string currents," *Energy Convers. Manage.*, vol. 178, pp. 250–264, 2018.

[6] A. Ramyar, H. Iman-Eini, and S. Farhangi, "Global maximum power point tracking method for photovoltaic arrays under partial shading conditions," *IEEE Trans. Ind. Electron.*, vol. 64, no. 4, pp. 2855–2864, Apr. 2017.

[7] L. Zhou, Z. Wu, G. Wang, and M. Wu, "An intelligent fuzzy controller for maximum power point tracking in partially shaded photovoltaic systems," in *Proc. 7th Int. Conf. Int. Hum.-Mach. Syst.*, Hangzhou, China, 2015, pp. 345–348.

[8] C.-L. Kuo, J.-L. Chen, S.-J. Chen, C.-C. Kao, H.-T. Yau, and C.-H. Lin, "Photovoltaic energy conversion system fault detection using fractional-order color relation classifier in microdistribution systems," *IEEE Trans. Smart Grid*, vol. 8, no. 3, pp. 1163–1172, May 2017.

[9] D. S. Pillai and N. Rajasekar, "A comprehensive review on protection challenges and fault diagnosis in PV systems," *Renew. Sustain. Energy Rev.*, vol. 91, pp. 18–40, Aug. 2018.

[10] M. K. Alam, F. Khan, J. Johnson, and J. Flicker, "A comprehensive review of catastrophic faults in PV arrays: Types, detection, and mitigation techniques," *IEEE J. Photovolt.*, vol. 5, no. 3, pp. 982–996, May 2015.

[11] K. A. Kim, G.-S. Seo, B.-H. Cho, and P. T. Krein, "Photovoltaic hot-spot detection for solar panel substrings using AC parameter characterization," *IEEE Trans. Power Electron.*, vol. 31, no. 2, pp. 1121–1130, Feb. 2016.

[12] Y. Zhao, J.-F. De Palma, J. F. Mosesian, and B. Lehman, "Line–line fault analysis and protection challenges in solar photovoltaic arrays," *IEEE Trans. Ind. Electron.*, vol. 60, no. 9, pp. 3784–3795, Sep. 2013.

[13] S. K. Firth, K. J. Lomas, and S. J. Rees, "A simple model of PV system performance and its use in fault detection," *Sol. Energy*, vol. 84, pp. 624–635, Apr. 2010.

[14] M. K. Alam and F. H. Khan, "PV faults: Overview, modeling, prevention and detection techniques," in *Proc. IEEE 14th Workshop Cont. Modeling Power Electron. (COMPEL)*, Salt Lake City, UT, USA, Jun. 2013, pp. 1–7.

[15] B. P. Kumar, G. S. Illango, M. J. B. Reddy, and N. Chilakapati, "Online fault detection and diagnosis in photovoltaic systems using wavelet packets," *IEEE J. Photovolt.*, vol. 8, no. 1, pp. 257–265, Jan. 2018.

[16] Z. Chen, L. Wu, S. Cheng, P. Lin, Y. Wu, and W. Lin, "Intelligent fault diagnosis of photovoltaic arrays based on optimized kernel extreme learning machine and I-V characteristics," *Appl. Energy*, vol. 204, pp. 912–931, Oct. 2017.

[17] R. Platon, J. Martel, N. Woodruff, and T. Y. Chau, "Online fault detection in PV systems," *IEEE Trans. Sustain. Energy*, vol. 6, no. 4, pp. 1200–1207, Oct. 2015.

[18] X. Lin, Y. Wang, M. Pedram, J. Kim, and N. Chang, "Designing fault-tolerant photovoltaic systems," *IEEE Design Test*, vol. 31, no. 3, pp. 76–84, Jun. 2014.

[19] A. Chouder and S. Silvestre, "Automatic supervision and fault detection of PV systems based on power losses," *Energy Conver. Manage.*, vol. 51, no. 10, pp. 1929–1937, Oct. 2010.

[20] M. Davarifar, A. Rabhi, A. El-Hajjaji, and M. Dahmane, "Real-time model base fault diagnosis of PV panels using statistical signal processing," in *Proc. Int. Conf. Renew. Energy Res. Appl. (ICRERA)*, Madrid, Spain, 2013, pp. 599–604.

[21] N. Gokmen, E. Karatepe, S. Silvestre, B. Celik, and P. Ortega, "An efficient fault diagnosis method for PV systems based on operating voltage-window," *Energy Conver. Manage.*, vol. 73, pp. 350–360, Sep. 2013.

[22] Syafaruddin, E. Karatepe, and T. Hiyama, "Controlling of artificial neural network for fault diagnosis of photovoltaic array," in *Proc. 16th Int. Conf. Intell. Syst. Appl. Power Syst.*, Hersonissos, Greece, Sep. 2011, pp. 1–6. [Online]. Available: ieeexplore.ieee.org/stamp/stamp.jsp?tp=&arnumber=6082219

[23] E. Garoudja, A. Chouder, K. Kara, and S. Silvestre, "An enhanced machine learning based approach for failure detection and diagnosis of PV systems," *Energy Convers. Manage.*, vol. 151, pp. 496–513, Nov. 2017.

[24] Z. Yi and A. H. Etemadi, "Line-to-line fault detection for photovoltaic arrays based on multi-resolution signal decomposition and two-stage support vector machine," *IEEE Trans. Ind. Electron.*, vol. 64, no. 11, pp. 8546–8556, Nov. 2017.

[25] Y. Zhao, R. Ball, J. Mosesian, J.-F. de Palma, and B. Lehman, "Graph-based semi-supervised learning for fault detection and classification in solar photovoltaic arrays," *IEEE Trans. Power Electron.*, vol. 30, no. 5, pp. 2848–2858, May 2015.

[26] S. Zhang, Y. Wang, M. Liu, and Z. Bao, "Data-based line trip fault prediction in power systems using LSTM networks and SVM," *IEEE Access*, vol. 6, pp. 7675–7686, 2018.

[27] R. Zhao, J. Wang, R. Yan, and K. Mao, "Machine health monitoring with LSTM networks," in *Proc. 10th Int. Conf. Sens. Tech. (ICST)*, Nanjing, China, 2016, pp. 1–6.

[28] L. Chen, S. Li, and X. Wang, "Quickest fault detection in photovoltaic systems," *IEEE Trans. Smart Grid*, vol. 9, no. 3, pp. 1835–1847, May 2018.

[29] T. Sen, P. Nataraj, V. Argawal, and R. Kumar, "Global maximum power point tracking of PV arrays under partial shading conditions using a modified particle velocity-based PSO technique," *IET Renew. Power Genrat.*, vol. 12, no. 5, pp. 555–564, Dec. 2017.

[30] W. Kong, Z. Y. Dong, Y. Jia, D. J. Hill, Y. Xu, and Y. Zhang, "Short-term residential load forecasting based on LSTM recurrent neural network," *IEEE Trans. Smart Grid*, vol. 10, no. 1, pp. 841–851, Sep. 2017.

[31] L. Yu, J. Chen, G. Ding, Y. Tu, J. Yang, and J. Sun, "Spectrum prediction based on Taguchi method in deep learning with long short-term memory," *IEEE Access*, vol. 6, pp. 45923–45933, 2018.

[32] S. Hochreiter and J. Schmidhuber, "Long short-term memory," *Neural Comput.*, vol. 9, no. 8, pp. 1735–1780, 1997.

[33] C. Lin *et al.*, "Early diagnosis and prediction of sepsis shock by combining static and dynamic information using convolutional-LSTM," in *Proc. IEEE Int. Conf. Healthcare Informat. (ICHI)*, New York, NY, USA, Jun. 2018, pp. 219–228.

[34] D. L. Marino, K. Amarahinghe, and M. Manic, "Building energy load forecasting using deep neural networks," in *Proc. IECON 42nd Annu. Conf. IEEE Ind. Electron. Soc.*, Florence, Italy, 2016, pp. 7046–7051.

[35] L. Zhang, H. Huang, and X. Jing, "A modified cyclostationary spectrum sensing based on softmax regression model," in *Proc. 16th Int. Symp. Commun. Inf. Technol. (ISCIT)*, Qingdao, China, 2016, pp. 620–623.
[36] D. Lin, Z. Lin, L. Sun, K.-A. Toh, and J. Cao, "LLC encoded BoW features and softmax regression for microscopic image classification," in *Proc. IEEE Int. Symp. Circuits Syst. (ISCAS)*, Baltimore, MD, USA, May 2017, pp. 1–4. doi: 10.1109/ISCAS.2017.8050243.
[37] S. Tao, T. Zhang, J. Yang, X. Wang, and W. Lu, "Bearing fault diagnosis method based on stacked autoencoder and softmax regression," in *Proc. 34th Chin. Control Conf.*, Hangzhou, China, Jul. 2015, pp. 6331–6335.
[38] K. Ishaque, Z. Salam, and H. Taheri, "Accurate MATLAB simulink PV system simulator based on a two-diode model," *J. Power Electron.*, vol. 11, no. 2, pp. 179–185, 2011.
[39] C. L. Nkashama, "Maximum power point tracking algorithm for photovoltaic home power supply," M.S. thesis, Dept. Elect. Eng., Univ. KwaZulu-Natal, South Africa, Durban, 2011, pp. 1–149.
[40] Q. Zhao, S. Shao, L. Lu, X. Liu, and H. Zhu, "A new PV array fault diagnosis method using fuzzy C-mean clustering and fuzzy membership algorithm," *Energies*, vol. 11, pp. 1–21, Jan. 2018.
[41] C.-S. Hsu and J.-R. Jiang, "Remaining useful life estimation using long short-term memory deep learning," in *Proc. IEEE Int. Conf. Appl. Syst. Invention (ICASI)*, Chiba, Japan, Apr. 2018, pp. 58–61.

ALBERT YAW APPIAH received the B.Sc. and M.Sc. degrees from the University of Mines and Technology, Tarkwa, Ghana, in 2007 and 2014, respectively. He is currently pursuing the Ph.D. degree with Nanjing Tech University, Nanjing, China. He is also a Lecturer with the Electrical/Electronic Engineering Department, Sunyani Technical University. His current research interests include solar photovoltaics, deep learning, fault diagnosis, and robotics.

XINGHUA ZHANG was born in Yushan, China, in 1963. He received the B.S. degree in physics from Jiangxi Normal University, Nanchang, China, in 1983, the M.E. degree in industry automation from Jiangnan University, Wuxi, China, in 1998, and the Ph.D. degree in control theory and engineering from Southeast University, Nanjing, China, in 2002. He is currently a Professor with the School of Electrical Engineering and Control Science and also the Head of the Institute of Electric Machine and Electrical Driving Control, Nanjing Tech University. His research interests include electric machines and driving control, nonlinear control theory, and multi-objective optimization algorithms.

BEN BEKLISI KWAME AYAWLI received the B.Ed. degree in information technology from the University of Education, Winneba, Ghana, in 2008, and the M.Sc. degree in information technology from Sikkim Municipal University, India, in 2011. He is currently pursuing the Ph.D. degree in automation with Nanjing Tech University, Nanjing, China. From 2013 to 2016, he was the ICT Director with Sunyani Technical University, Ghana, where he is currently a Lecturer with the Computer Science Department and also a Web Application Developer. His research interests include machine learning, mobile robot path planning and navigation, data mining, and web applications.

FRIMPONG KYEREMEH received the bachelor's degree in technology education from the University of Education, Winneba, Ghana, in 2005, and the M.Sc. degree in electrical engineering with power electronics from Bradford University, U.K., in 2008. He is currently pursuing the Ph.D. degree in electrical engineering and control science with Nanjing Tech University, China. He is also a Lecturer with the Electrical/Electronic Engineering Department, Sunyani Technical University, where he taught courses on basic electronics, power electronics, engineering practice, and power systems. His current research interests include microgrid control, machine learning, and multi-agent systems.